Optics Communications 537 (2023) 129441

Contents lists available at ScienceDirect

Optics Communications

journal homepage: www.elsevier.com/locate/optcom

Broadband supercontinuum generation in cascaded tapered liquid core fiber

Lanh Chu Van [a], Ngoc Vo Thi Minh [a], Bao Tran Le Tran [a], Trong Dang Van [a], Phuong Nguyen Thi Hong [a], Trang Do Mai [a], Trung Le Canh [a], Hieu Van Le [b], Thuy Nguyen Thi [c], Thanh Thai Doan [d], Van Thuy Hoang [a,*]

[a] Department of Physics, Vinh University, 182 Le Duan, Vinh City, Viet Nam
[b] Faculty of Natural Sciences, Hong Duc University, 565 Quang Trung Street, Thanh Hoa City, Viet Nam
[c] University of Education, Hue University, 34 Le Loi, Hue City, Viet Nam
[d] Ho Chi Minh City University of Food Industry, 140 Le Trong Tan, Tan Phu, Ho Chi Minh City, Viet Nam

ARTICLE INFO

Keywords:
Optical fiber
Nonlinear fiber
Supercontinuum generation
Coherence
Tapered fiber
Liquid core fiber
Group velocity dispersion

ABSTRACT

Most recent broad supercontinuum sources have used nonlinear fibers with small core diameters, resulting in low coupling efficiency, limiting power level launching into the fiber, and low spectral power density. In this work, we numerically investigate tapered liquid-core fibers for supercontinuum generation that have a potential for both high coupling efficiency (with a standard SMF-28 fiber) and high nonlinear effects. Carbon disulfide is selected to fill into the fibers because of its high nonlinear refractive index and high transparency from the visible to the mid-infrared range. We consider cascaded fibers including SMF-28 and the tapered liquid-core fibers for all-normal and anomalous dispersion supercontinuum generation pumped by C-band femtosecond lasers (1560 nm, 90 fs). In such a case, we obtain all-normal dispersion supercontinuum generation with flat-top, broad bandwidth (1.0–2.5 μm) via an input peak power of 27 kW. By changing the core diameter of the tapered fiber, we also yield anomalous dispersion supercontinuum generation with broad spectral bandwidth (1.0–3.3 μm). In addition, the use of the cascaded tapered fibers is possible to mitigate fiber damage (via thermal effects of a high-power laser on the selected liquids) and increase stability of output supercontinuum spectra. In this context, supercontinuum generation in the cascaded fibers by using a picosecond laser with high average power (≈ 800 mW) is considered towards applications requiring high spectral power density (e.g., multiphoton imaging techniques).

1. Introduction

Fiber-based supercontinuum (SC) sources have played a significant role in science and industry via their unique properties, i.e., brightness, multi-octave frequency spanning, single-mode output, and high spatial and temporal coherence. The important applications of fiber-based SC sources include, for example, frequency combs [1], material processing, optical sensing, absorption spectroscopy [2], and metrology [3]. In the near and short-wavelength infrared, SC sources with spectral bandwidth covering numerous multi-photon absorption peaks of vast fluorophores have motivated multi-photon microscopy for imaging living tissues with large penetration depth [4,5]. Coherent SC generation covering the major gain bands of rare-earth amplifiers has been used as coherent seeds for low-noise ultrafast fiber lasers [6]. For the last few years, it has seen attractive research to improve the spectro-temporal properties of SC sources, such as extending spectral spanning — from deep ultra-violet (UV) up to mid-infrared (IR), upgrading the output spectrum stability, "on-the-fly" controlling the properties of SC generation leveraging machine learning and deep learning techniques [5,7–9].

It is worth mentioning that silica-based fibers have been used widely for SC generation, and they can provide SC spectra with spectral broadening in a range of 0.4–2.4 μm and watt-level of output average power. Extending the SC bandwidth leads to the necessary development of non-silica fiber materials, such as gases, liquids, or hybrid glasses. The gas-core fibers (i.e., hollow-core fiber infiltrated with notable gases) have typically been used for SC generation in UV and visible range [10]. They are applicable in ultrafast molecular spectroscopy [11] and coherent anti-stokes Raman scattering (CARS) microscopy [4]. Notwithstanding, the drawbacks of gas-core fibers are the narrow transmission bandwidth if antiresonant and/or band-gap fibers are used. The light also can be guided in a hollow core microcapillary filled with a gas. However, the core diameter of the capillary must be large (a few hundred micrometers) to reduce the loss, thus an extremely high input pulse energy (at a level of μJ) is required for broad SC generation [12]. The gas-core fibers also require a complex experimental setup with

* Corresponding author.
E-mail address: thuyhv@vinhuni.edu.vn (V.T. Hoang).

https://doi.org/10.1016/j.optcom.2023.129441
Received 20 December 2022; Received in revised form 12 March 2023; Accepted 15 March 2023
Available online 17 March 2023

the use of gas cells, vacuum equipment to operate, and high-power lasers as pump sources. Another approach is to use soft-glass fibers made from fluoride, chalcogenide, and telluride [7,13–17] for SC in the mid-IR range. They have found applications in optical coherence tomography (OCT) imaging, security, medical surgery, remote sensing, and air pollution monitoring [18,19]. However, the soft-glass fibers have weak-mechanic resistance, and high loss via crystallization. The soft-glass fibers also require harmonic processes and/or an optical parametric oscillator and amplifier to adjust pump wavelengths to match with dispersion characteristics for broadband SC generation [20]. In addition, both gas-core fibers and soft-glass fibers are incompatible with standard fiber technology in fiber coupling by using conventional fusion splicer, which limits development of a compact all-fiber system for SC generation.

Recently, liquid-core fibers have emerged as a versatile solution to overcome the aforementioned challenges [21–23]. In particular, the selected liquids, such as carbon disulfide (CS_2), carbon tetrachloride, and toluene, have a high nonlinear refractive index [24,25] and optical transparency in the near and mid-IR range [26]. Thus, liquid-core fibers can offer multi-octave broadband SC generation (from visible up to mid-IR range) by using standard commercial femtosecond lasers as pump sources [27–30]. Moreover, unlike solid-core fibers where the optical properties are almost constant via changing of ambient temperature and pressure, the sensitivity to temperature of the selected liquid enables real-time controlling of the properties of liquid-core fibers (e.g., dispersion, mode guidance). This provides a high degree of freedom to optimize the spectro-temporal characteristics of SC generation for practical applications [29]. The drawback of liquid core fibers is requiring a complex experimental setup system using a liquid reservoir to fill the selected liquid into the fiber core and fully keep liquids in the fiber core [21,22,29].

Up to now, almost all of the liquid core fibers considered for SC generation have a small core diameter (on the level of single-digit micrometers or even smaller) to enhance the nonlinear coefficient via the small effective mode area [22],[28–33], and single-mode guidance. The small core fibers also allow to efficiently adjust the fiber properties (dispersion regime, position of zero-dispersion wavelength, loss, polarization) by changing the cladding structure (i.e., diameter and pitch lattice of the cladding air-holes). However, the small core fibers typically offer a low coupling efficiency with the standard single-mode fibers if an all-fiber system is considered for SC generation. It is to note that coupling efficiency between two fibers depends on the coupler, and fiber properties (e.g., polarization, overlap between the mode exited in the fibers). Typically, two fibers with similar effective mode areas provide high coupling efficiency between them [34]. Therefore, in another approach, a few of the previous works considered large core photonic crystal fibers (PCFs) infiltrated with liquids for SC generation [21,35]. The aim of using these fibers is to assure a high coupling efficiency with the selected laser source and standard single-mode fibers. However, large core PCFs have a limitation in optimizing mode properties to match with properties of used laser sources. The large core fibers also have a low nonlinear coefficient, and thus, a high peak power of input laser pulses is needed for broad SC generation. Therefore, the development of a liquid-core fiber that can provide both a high nonlinear coefficient and coupling efficiency with a standard single-mode fiber is necessary to improve and widen the application range of fiber-based SC sources.

In order to meet this requirement, tapered fibers have been used as a versatile approach for broad SC generation [36–40] because of their unique configuration. Particularly, the untapered part with a large mode area guarantees an efficient input coupling, and the waist part with a small core (i.e., a small mode area) can provide a high nonlinear coefficient resulting in readily spectral broadening. Moreover, the tapering process to scale-down fiber cross-section enables changing the mode properties, e.g., dispersion, and birefringence, so that to finely match with a central wavelength of the laser sources and application requirements. For instance, the tapered process can shift the dispersion from the anomalous to normal dispersion regime, thus tapered fibers have been leveraged for the all-normal dispersion (ANDi) SC generation with high coherence and flat-top output SC spectrum in the ultraviolet, visible [41], or mid-IR range [40]. However, state-of-the-art tapered fibers are mostly based on solid-core fibers. The combination of advantages of liquid-core and tapered fiber is necessarily exploited for a robust compact all-fiber SC system.

In this work, we numerically demonstrate the SC generation in cascaded tapered liquid core fiber. In particular, the liquid core is a capillary with a large core diameter of 14 μm infiltrated with CS_2. The large core is used for high coupling efficiency with standard single-mode fiber and/or large-mode area fibers for high-power laser delivery [42,43]. The mode properties (dispersion, loss, effective mode area) of tapered fibers are calculated by using the finite-difference eigenmode method. Next, the spectro-temporal properties of SC generation in the cascaded tapered fibers are characterized by using the split-step method with a standard commercial femtosecond Erbium laser as a pump source.

Table 1
Length of tapered fiber. $\#F_1$ and $\#F_2$ indicate the tapered fibers considered in this work with waist diameter d_3 = 3 μm and 2.5 μm, respectively.

Fiber part	Length (cm)	Core diameter (μm)
Input-light untapered (d_1)	1	14
Down-tapered transition (d_2)	1	14 → 3 (for $\#F_1$); 14→2.5 (for $\#F_2$)
Waist (d_3)	2	3 (for $\#F_1$) and 2.5 for ($\#F_2$)
Up-tapered transition (d_4)	1	3 → 14 (for $\#F_1$); 2.5→14 (for $\#F_2$)
Output-light untapered (d_5)	5	14

2. Fiber design

Schemes of the tapered fiber are presented in Fig. 1. The fiber is a step-index, and it is made by tapering a silica micro-core capillary. Carbon disulfide is subsequently infiltrated into the core for light guidance. From an experimental perspective, the silica capillary can be tapered by using the heating-and-stretching method or tapering cold-and-fast [44–47]. It also can be directly drawn from a draw tower which offers high accuracy of the fiber parameters by changing temperature and pressure during the fiber-draw process [48]. The liquid infiltration may be implemented by using a liquid pump system [21,35]. In such a system, the selected liquid is filled into the core of the capillary by capillary force and pressure from a microfluidic pump. The coupling between the proposed liquid core fiber with a single-mode fiber can be carried out by using an alignment sleeve [49] or a conventional fusion splicer [50]. The length of the proposer fiber is shown in Table 1.

In this work, we conserved carbon disulfide (CS_2) for a light guidance medium (i.e., the core of the proposed fibers). CS_2 is toxic which may limit the possibility of the proposed fibers for practical applications. However, in comparison with other liquids, this liquid has a relatively high nonlinear refractive index, high transparency from visible up to 4 μm [25,26]. Moreover, carbon disulfide has a refractive index higher than that of silica to guarantee light guidance by total internal reflection with low leakage loss. Properties of CS_2 and silica, as shown in Fig. 2, are used to calculate linear properties of the tapered fibers. Both silica and CS_2 have high attenuation in the mid-IR range ($\lambda > 2.8$ μm), see Fig. 2(b), this may decrease output intensities of SC generation and limit the spectral broadening in the mid-IR range.

The full-vectorial finite-difference method with the perfectly matched layer (PML) boundaries is used to calculate the linear properties of the proposed fibers, where the calculated region is a rectangular (50 × 50 μm) with a size of the mesh step is 0.1 μm. Fig. 3 presents the advantages of tapered fiber that allow not only tailoring dispersion profiles but also reducing effective mode areas (i.e., increasing nonlinear coefficient). For example, the untapered parts have effective

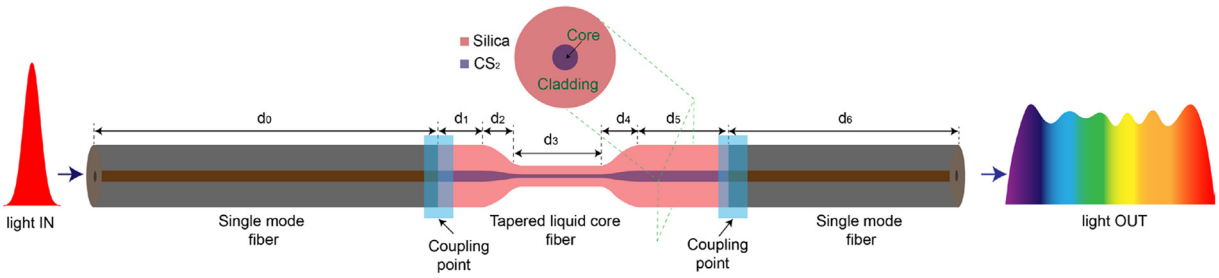

Fig. 1. Scheme of a cascaded liquid core fiber for broad supercontinuum generation.

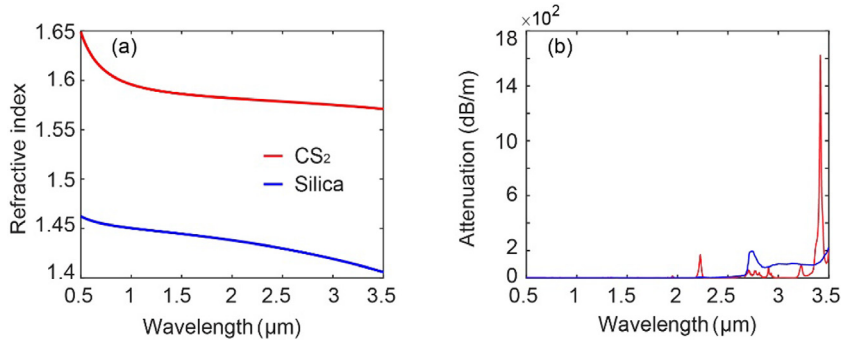

Fig. 2. (a) Refractive index of CS_2 [22] and silica [51], (b) material attenuation of CS_2 [26] and silica [51].

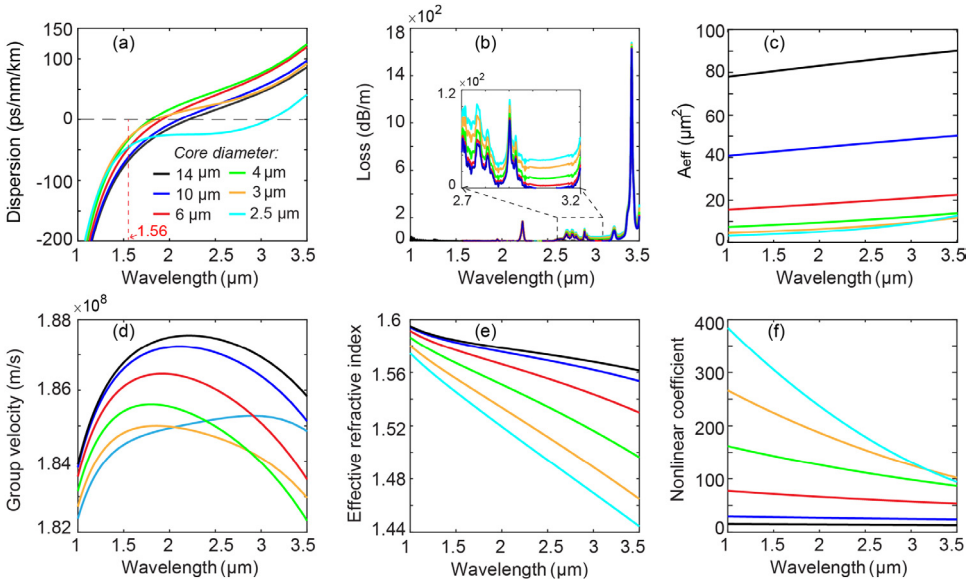

Fig. 3. Linear properties of tapered fibers at considered cross-sections with various core diameters. (a) group-velocity dispersion, (b) loss, (c) effective mode area, (d) group velocity, (e) effective refractive index, (f) nonlinear coefficient.

mode areas (A_{eff}) of 78-90 μm^2 and nonlinear coefficients (γ) of 12–15 (W^{-1} km^{-1}), while the waist part (with d_{core} = 2.5 μm) has A_{eff} of 3.15–12.8 μm^2 and γ of 94–384 (W^{-1} km^{-1}), see Fig. 3 (c, f).

The fiber has a core diameter (d_{core}) of untapered parts of 14 μm, and the core diameter is tapered down to around 2.5 μm or 3 μm by the tapering process. The large core of untapered parts assures high coupling efficiency between tested fiber with standard silica fiber. For example, we numerically calculate the coupling efficiency between the proposed fiber and SMF-28 by 90% (i.e., 0.45 dB of coupling loss). The diameter of the waist part at 2.5 μm assures all-normal near-zero dispersion in the investigated wavelength range (from 1 μm to 3 μm), see Fig. 3(a), and thus, this fiber can be used for all-normal dispersion SC generation (ANDi). Whilst, the waist part with a core diameter of 3 μm has flat dispersion profiles with zero-dispersion wavelength (ZDW) at 1.8 μm, and this fiber is used for soliton-induced SC generation that typically has broader spectral bandwidth than the ANDi SC generation via the same level of input laser power.

The fiber dispersion depends on the material dispersion of CS_2, silica, as well as waveguide dispersion as shown in previous works [52,53]. However, the waveguide dispersion has a significant influence on the fiber dispersion if the fiber has a small core in comparison with the wavelength (e.g., $d_{core}/\lambda < 2$). Thus, the fiber with a large core has a dispersion shape following material dispersion of the core material (i.e., CS_2). Because of the significant influence of waveguide dispersion,

the small core fiber (d_{core} = 2.5 μm) has flat dispersion and ZDW at 3 μm, while the fiber with d_{core} = 3 μm has the dispersion shape with high slope and ZDW at 2 μm.

Losses of the proposed fibers include confinement loss and material loss of CS_2 in the core as well as silica in the cladding. Since CS_2 has higher refractive index than silica, the light is strongly confined inside the core resulting in low confinement loss. Consequently, loss profiles of fibers with various core diameters follow the material attenuation of CS_2, see Fig. 3(b). However, in the mid-IR range, a fiber with a small core diameter (e.g., d_{core} = 2.5 μm) has a loss slightly higher than a large core fiber (e.g., d_{core} = 14 μm), see inset in Fig. 3(b). The higher loss of the small core fiber originates from confinement and high absorption of silica in the mid-IR range.

The tapered fibers, theoretically, support multimode guidance. Notwithstanding, in our model, we assume that only the fundamental mode (LP''_{01}) is exited. It is also to note that large walk-off between the modes in step-index fibers, as well as the use of subpicosecond laser pulses, and short fiber lengths, enable a significant reduction of nonlinear interaction between the modes, and thus, effects of high order modes on the nonlinear propagation can be neglected [54,55]. During nonlinear propagation along the tapered fibers, the mode properties of LP_{01} are gradually changed, including dispersion, loss, mode area, delay, and phase. Therefore, along with dispersion and nonlinear effects, the terms for the delay (described by group velocity) and phase (described by effective refractive index) would be considered as shown in Eq. (1) in the below section. The values of group velocity and effective refractive index are shown in Fig. 3 (d,e).

In this work, we consider two kinds of tapered fibers for anomalous and ANDi SC generation. These fibers are labeled as $\#F_1$ and $\#F_2$ with waist diameters (d_3) of 3 μm and 2.5 μm, respectively.

3. SC generation in tapered fibers

3.1. Numerical modeling

SC generation in cascaded tapered liquid-core fibers is numerically simulated by solving the general nonlinear Schrodinger equation (GNLSE) as given in Eq. (1):

$$\frac{\partial A}{\partial z}+\frac{\alpha(z)}{2}A-i\left[\beta_0(0)-\beta_0(z)\right]A+\left[\beta_1(0)-\beta_1(z)\right]\frac{\partial A}{\partial T}-\sum_{k\geq 2}\frac{i^{k+1}}{k!}\beta_k(z)\frac{\partial^k A}{\partial T^k}=i\gamma(z)\left(1+i\tau_{shock}\frac{\partial}{\partial T}\right)\times\left\{(1-f_R)|A|^2A+f_RA\int h(T-T')\left|A(T-T')\right|^2dT'\right\} \quad (1)$$

where $A(z,T)$ is amplitude function of input pulse, $\alpha(z)$ is the loss, $\beta_k(z)$ ($k \geq 2$) is the first and high-order dispersion. In our model, we calculate with dispersion terms with k = 41. T is the retarded time frame comoving with A given by $T = t\text{-}z\beta_1(0)\beta_0$ *and* β_1 are calculated by effective refractive index (n_{eff}) and group velocity (v_g) as given in Eq. (2):

$$\beta_0(z)=\frac{2\pi}{\lambda}n_{eff}(z)\ \text{and}\ \beta_1(z)=\frac{1}{v_g(z)} \quad (2)$$

$\tau_{shock} = 1/\omega_0$ is the shock time regarding the self-steepening effect. Nonlinear coefficient γ is determined through effective mode area and nonlinear refractive index, $\gamma(z)=\frac{2\pi n_2}{\lambda A_{eff}(z)}$ in which n_2 is the nonlinear refractive index. The value of the nonlinear refractive of CS_2 is in the range of 2×10^{-19} –30×10^{-19} m^2/W, depending on the pulse duration of the excitation laser [25].

$h(T)$ is the response Raman function which is determined from the nonlinear mechanism of CS_2 [24,25], such as reorientation, interaction, and collision-induced of CS_2 molecules via effects of external electromagnetic fields. $h(T)$ is approximately a sum of the commend nonlinear mechanism as given in Eq. (3):

$$h(T)=\frac{1}{N_2}\left(n_{2l}e^{-T/t_{f,l}}\int_0^\infty\frac{\sin(\omega T)}{\omega}g(\omega)\,d\omega+\sum_{k=c,d}n_{2k}\left(1-e^{-T/t_{r,k}}\right)e^{-T/t_{f,k}}\right) \quad (3)$$

where the subscripts *d, l, c* indicate the molecular reorientation, molecular interaction, and collision-induced, respectively, and $N_2 = n_{2d}+n_{2l}+n_{2c}$. Values of nonlinear parameters of CS_2 are shown in Table 2.

Table 2
Values of nonlinear parameters of CS2 [25].

Parameters	Values	Parameters	Values
$n_{2d}(10^{-19}$ $m^2/W)$	18	$t_{r,c}$ (ps)	0.15
$n_{2l}(10^{-19}$ $m^2/W)$	7.6	$t_{f,c}$ (ps)	0.14
$n_{2c}(10^{-19}$ $m^2/W)$	1.0	$t_{f,l}$ (ps)	0.45
$t_{r,d}$ (ps)	0.15	ω_0 (ps^{-1})	8.5
$t_{f,d}$ (ps)	1.61	σ (ps^{-1})	5

In our model, we consider shot-to-shot coherence via the effects of vacuum noise [56] and laser noise (i.e., amplitude fluctuation of each laser pulse compared to mean values) [57,58]. The formation of input pulses is written in Eq. (4) [57].

$$A(0,t)=\sqrt{P_0}\delta_{AN}\,\text{sech}\left(\frac{t}{\left(T_0\left(1-0.8\left(\delta_{AN}-1\right)\right)\right)}\right)+F^{-1}\left(\delta_{QN}\right) \quad (4)$$

Where P_0 is the peak power, T_0 is the pulse duration, δ_{AN} is a single random value for each input pulse with unit mean and its a standard deviation equal to the root mean square (RMS) amplitude noise of the modeled laser (RMS = 0.5% for our model, i.e., RMS of C-band femtosecond laser [59]). F^{-1} is inverse Fourier transform. δ_{QN} is the phase noise of the input pulse over each spectral bin with angular frequency ω_m as given in Eq. (5) [57].

$$\delta_{QN}=\left(\sqrt{\frac{h\omega_m}{\Delta\Omega}}\right)\exp\left(i2\pi\Phi_m\right) \quad (5)$$

where h is Planck's constant and Φ_m is a random number Gaussian distributed in the interval [0,1]. Φ_m is also a random phase in each spectral bin ω_m and bin size $\Delta\Omega$.

The equation to calculate the coherence is given in Eq. (6) [60]:

$$\left|g_{12}^{(1)}(\omega)\right|=\left|\frac{\left\langle\widetilde{A}_i^*(\omega)\,\widetilde{A}_j(\omega)\right\rangle_{i\neq j}}{\left[\left\langle\left|\widetilde{A}_i(\omega)\right|^2\right\rangle\left\langle\left|\widetilde{A}_j(\omega)\right|^2\right\rangle\right]^{\frac{1}{2}}}\right| \quad (6)$$

In this work, we use parameters of a pump laser which are extracted from a commercial C-band laser (central wavelength at 1560 nm, pulse duration of 90 fs and 1 ps). For ultrashort pulses (90 fs), CS_2 has a nonlinear refractive index is around of 3×10^{-19} m^2/W, and the Raman fraction (f_R) is 0.5 [24,25]. Whilst, for picosecond laser pulses, CS_2 has a nonlinear refractive index is around 20×10^{-19} m^2/W, and the Raman fraction (f_R) is 0.95 [25]. The nonlinear propagation in a noninstantaneous Kerr (i.e., duration-dependent Kerr nonlinearity and Raman factors) is also thoroughly theoretically investigated in ref [61].

3.2. Femtosecond anomalous dispersion SC generation

$\#F_1$ fiber with a waist diameter of 3 μm has group velocity dispersion changing along the fiber and zero-dispersion wavelength varies in the range of 1.7–2.2 μm (depending on the diameter of the fiber part). Therefore, $\#F_1$ fiber can offer broad bandwidth SC generation via soliton dynamics. Fig. 4 presents nonlinear propagation in 10 cm of $\#F_1$ fiber with input energy of 1.5 nJ (peak power of 27 kW) and pulse duration of 90 fs. The input pulse is almost spectrally broadened in the waist part, and the spectral structure of the pulse does not noticeably change during further propagation in the up-tapered transition (d_4) and untapered part (d_5), see Fig. 4(b). Evolution of the pulses in the time domain is shown in Fig. 4(a). Most input pulse energy locates in the normal dispersion regime with a smooth temporal profile, i.e., positive

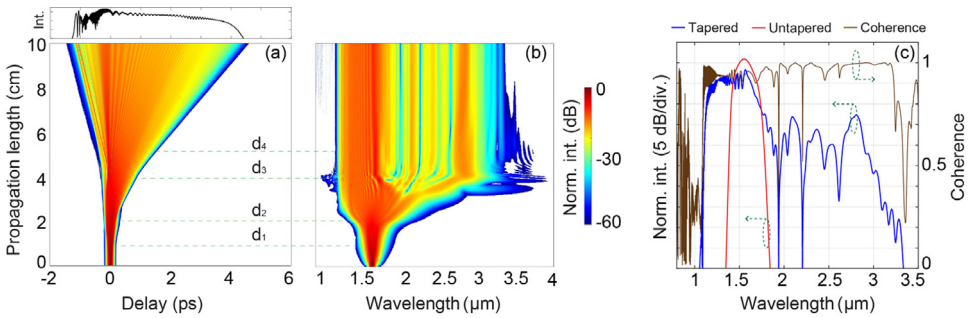

Fig. 4. Pulse evolution in #F$_1$ fiber. (a) evolution of the input pulse in the time domain and the inset shows temporal profile at 10 cm of propagation, (b) spectral evolution, (c) coherence and spectrum at 10 cm of propagation in $\#F_1$ fiber and untapered fiber (uniform fiber).

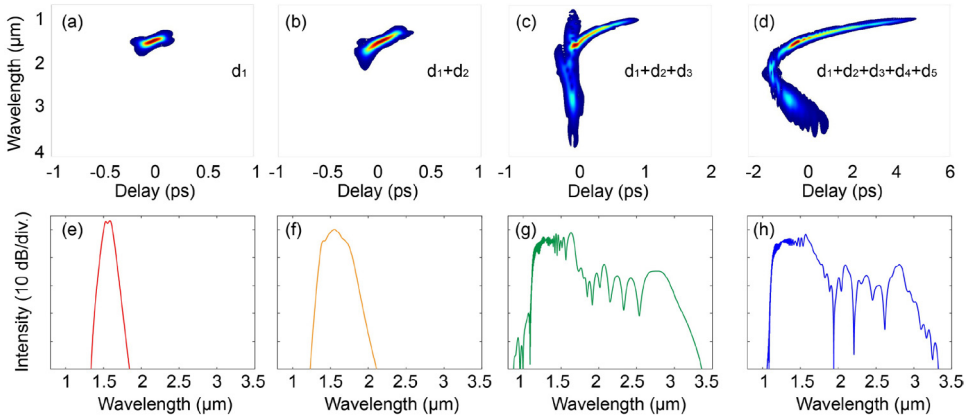

Fig. 5. Spectrogram and spectrum at the end of various parts of #F$_1$ fiber. (a, e) input-light untapered part, (b, f) down-tapered part, (c, g) waist part, and (d, h) output-light untapered part.

delay. Meanwhile, the spectral components of solitons in the anomalous dispersion regime have negative delay. The output SC spectrum has a spectral bandwidth of 1.1–3.3 μm within 30 dB, the spectral bandwidth is much broader than that obtained from untapered (uniform) fiber, see Fig. 4(c).

The SC generation is high coherence with $\left|g_{12}^{(1)}(\omega)\right| \approx 1$ over most wavelength bits of the SC spectrum. The high coherence can be understood by noting that the SC generation is induced by SPM at the beginning of propagation in normal dispersion regime and a small part of the spectrum is to form solitons in anomalous dispersion regime when SMP-induced spectrum excess ZDWs. In this context, modulation instability does not play a significant role in amplifying the vacuum noise, thus the SC generation exhibits high coherence.

Nonlinear dynamics for spectral broadening are in detail described in Fig. 5. SPM is the main contribution to nonlinear propagation in the input-light untapered part (d_1). The large effective mode area (i.e., low nonlinearity) leads to narrow spectrum bandwidth in this part, see Fig. 5 (a, e). The smooth decrease of core diameter in the down-tapered part leads to further spectral broadening, however, the spectrum is still in normal dispersion regime and no soliton is formed, Fig. 5 (b, f). In the tapered waist, spectral broadening could exceed ZDW at 1.75 μm resulting in soliton formation. Such soliton shifts toward long wavelengths via self-frequency soliton shifting, contributing to spectral broadening at the leading edge of the pulse. Whilst, the structure of the trailing edge becomes further complex that consists of dispersive wave (DW) related to soliton shifting and OWB, see Fig. 5 (c, g). In the up-tapered and output-light untapered parts, large effective mode area (i.e., low nonlinear coefficient) restricts the soliton shifting as well as DW at the trailing edge. Consequently, no new wavelength is created during further propagation, and the spectrum structure at the end of the waist and untapered parts are similar to each other, see Fig. 5 (g, h). The spectrogram at the trailing edge experiences a normal dispersion regime, and thus, it is stretched out with further flatness for the wing, see Fig. 5(d).

The above study of nonlinear propagation in $\#F_1$ fiber is extended to investigate SC generation in a cascaded fiber with the same values of input laser (i.e., the central wavelength of 1560 nm, peak power of 27 kW, and pulse duration of 90 fs). The considered cascaded fiber is an all-fiber system as shown in Fig. 1 including input SMF-28 ($d_0 = 100$ cm), $\#F_1$ fiber, and output SMF-28 ($d_6 = 10$ cm). In our model, SMF-28 has $A_{eff} = 82\ \mu m^2$, dispersion $\beta_2 = -0.023$ ps^2/m and $\beta_3 = 1.47 \times 10^{-4}$ ps ^{3}/m. The loss SMF-28 is assumed to follow the material loss of silica with high transparency in visible and near-IR and high attenuation in the mid-IR range ($\lambda > 2.8$ μm).

High-order modes can be excited when the light from the SMF-28 launches into the liquid-core fiber, resulting in energy transfer from the fundamental mode to the excited high-order modes. However, as the above comment, the coupling efficiency depends on the effective mode area and polarization between the modes. In this context, we numerically calculate the coupling efficiency between the fundamental mode in the SMF-28 and high-order modes in the liquid core fiber. The results point out that the coupling efficiency between the fundamental mode in the SMF-28 and high-order modes in the liquid core is low, for example, the coupling efficiency between LP_{01} in the SMF-28 and LP_{02} mode in the liquid core fiber is 0.5%, whilst the coupling efficiency between LP_{01} in the SMF-28 and other high-order modes in the liquid-core fiber is close to zero. Therefore, we consider only the fundamental mode that is excited in the liquid core fiber for SC generation.

Evolution of the input pulse in a cascaded fiber is shown in Fig. 6. The narrow spectral broadening in the d_0 part (input-light SMF-28) includes a fundamental soliton (F) and DW. The soliton is slightly shifted to long wavelengths via self-frequency shifting, see Fig. 6(a). At 100 cm of the propagation, the soliton and DW have central wavelengths at 1680 nm and 1535 nm, respectively, see Fig. 6 (f, g). This leads to spectral broadening in the tapered fiber ($\#F_1$), which includes DW-induced

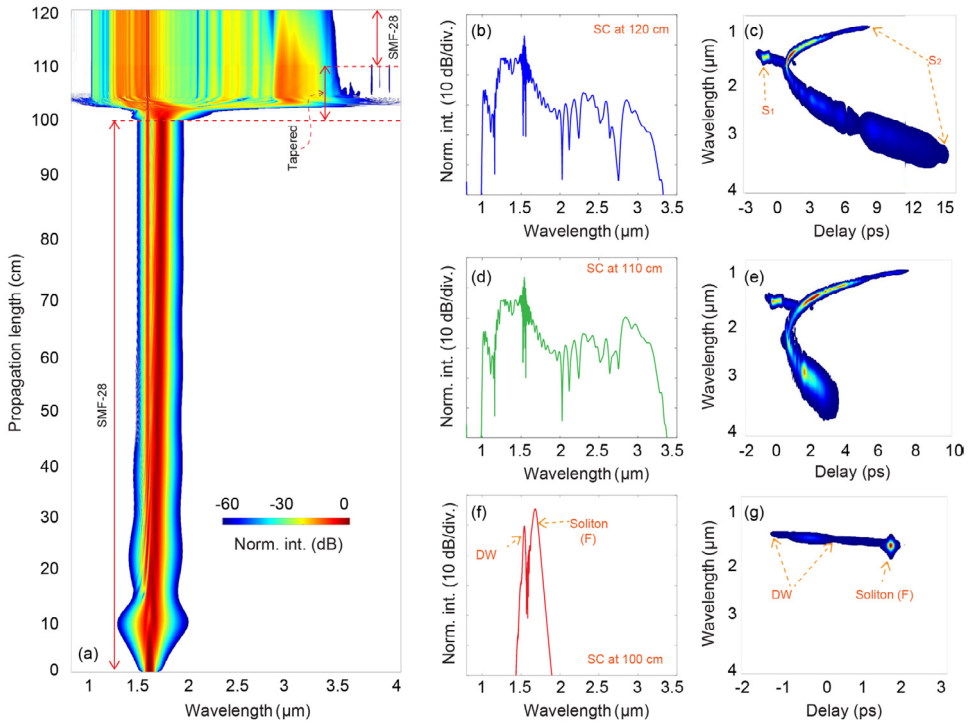

Fig. 6. (a) Evolution of the laser pulse in the cascaded fiber including input SMF-28, $\#F_1$ fiber, and output-SMF-28. (b, c) spectrum and spectrogram at the end of output-SMF-28, (d, e) the end of $\#F_1$ fiber, and (f, g) the end of the input SMF-28.

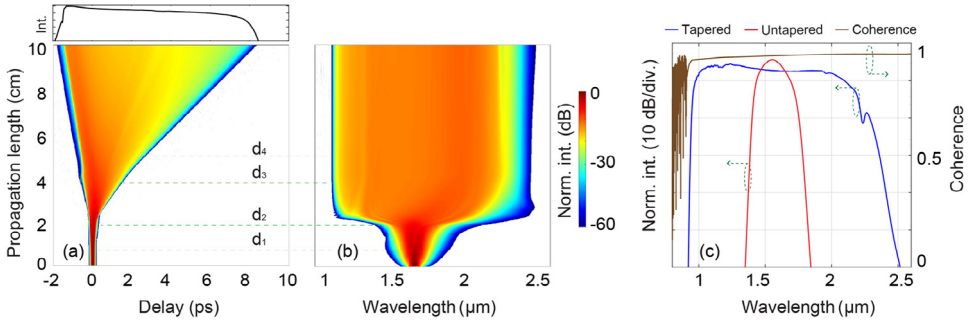

Fig. 7. Pulse evolution in $\#F_2$ fiber. (a) evolution of the input pulse in the time domain and the inset shows temporal profile at 10 cm of propagation, (b) spectral evolution, (c) coherence and spectrum at 10 cm of propagation in $\#F_2$ fiber and untapered fiber (uniform fiber).

(S_1) and soliton-induced (S_2). These parts have different delays, and they visibly separate each other in the time domain as shown in Fig. 6 (c, e). The spectral broadening in $\#F_1$ fiber is mainly induced by the soliton F because of its ultrashort pulse duration (around 60 fs) and peak power of 34.7 kW. Whilst, the DW in the d_0 has a pulse duration of 0.45 ps and peak power of 0.59 kW is slightly breaded by SPM during further propagation in the tapered fiber. At the end of the tapered fiber, SC has spectral bandwidth in the range of 1.0–3.3 μm within 30 dB dynamics.

The use of SMF-28 as an output fiber (d_6) of the cascaded fiber system leads to a significant decrease of light intensities at the long wavelengths (λ>2.8 μm) via strong absorption of silica, as shown in Fig. 6 (a,b). Therefore, the short length of output fiber (e.g., d_6 = 10 cm) should be used for the cascaded fiber system.

3.3. Femtosecond all-normal dispersion SC generation

The waist part with a core diameter of 2.5 μm has all-normal dispersion in the investigated wavelength range, thus spectral broadening mainly occurs in the normal dispersion regime. In the other words, ANDi SC generation can be observed in $\#F_2$ fiber.

Fig. 7 presents ANDi SC generation with an input peak power of 27 kW in $\#F_2$ fiber. The pulse is slightly broadened in the input-light untapered (d_1) and tapered-down part (d_2) because these parts have large effective mode areas (i.e., low nonlinearity). The spectral broadening mainly occurs in the waist parts by contributions of SPM and optical-wave breaking (OWB), see Fig. 7(b). Consequently, the output SC spectrum has an octave-spanning bandwidth of 0.94–2.3 μm within 20 dB dynamics. The ANDi SC in $\#F_2$ fiber is much broader than that in untapered fiber (i.e., longitudinal uniform structured fiber). In addition, since MI is suppressed in a normal dispersion regime, the ANDi SC, therefore, has high coherence over the whole observed spectrum, see Fig. 7(c). A single pulse is maintained in the time domain with a smooth temporal profile. The high values of normal dispersion in the short wavelengths lead to a large delay at the trailing edge, see Fig. 7(a).

Nonlinear dynamics of spectral broadening in $\#F_2$ fiber are further studied and shown in Fig. 8. The spectral broadening is completed in the tapered waist of the fiber because of the high nonlinear coefficient in this fiber part, see Fig. 8 (b, e). The spectral broadening is induced by SPM in the input untapered fiber (d_1) and tapered-down part (d_2) with a narrow spectral bandwidth and linear varying in time of the

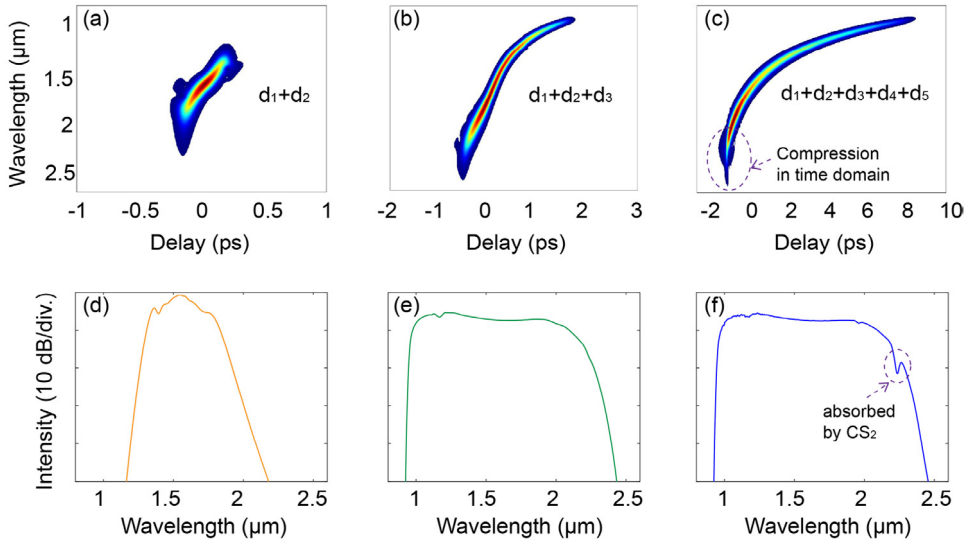

Fig. 8. Spectrogram and spectrum at the end of various parts of $\#F_2$ fiber. (a, d) down-tapered part, (b, e) waist part, and (c, f) output-light untapered part.

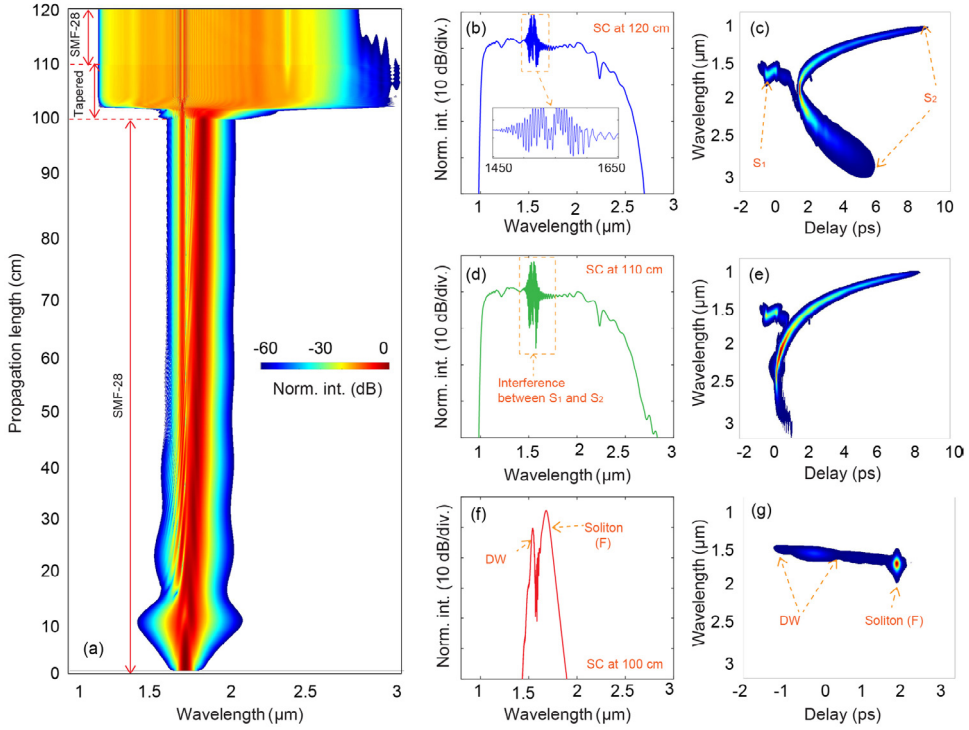

Fig. 9. (a) Evolution of the laser pulse in the cascaded fiber including input SMF-28, $\#F_2$ fiber and output-SMF-28. (b, c) spectrum and spectrogram at the end of output-SMF-28, (d, e) the end of $\#F_2$ fiber, and (f, g) the end of the input SMF-28.

instantaneous frequencies, see Fig. 8 (a, d). The OWB occurs firstly in the trailing edge of the pulse at 2.5 cm of propagation, and it creates new wavelengths around 1000 nm. In the leading edge, the low value of dispersion (i.e., flat and close to zero) leads to the unclear observation of OWB. During further propagation (in up-tapered and output-light untapered parts), no new wavelengths are created, and thus spectrum at the end of the waist (d_3) and output-light untapered part (d_5) have the same bandwidth (from 0.94 to 2.3 μm). The absorption peak of CS_2 at 2.2 μm decreases spectral intensity around this wavelength, see Fig. 8(f).

The spectrogram is further stretched out via effect group velocity dispersion in the time domain. In addition, it should be pointed out that the output-light untapered part has ZDW at 2.2 μm, and thus a part of the spectrum with $\lambda > 2.2$ μm moves in an anomalous dispersion regime. However, no soliton is formed herein because of not enough high energy. Notwithstanding, the anomalous dispersion causes slower movement of the long wavelengths than the short ones. Consequently, spectrograms of the leading edge (in anomalous dispersion regime) become further compressed, see Fig. 8(c).

SC generation in a cascaded fiber with $\#F_2$ fiber is shown in Fig. 9 with spectral bandwidth from 1.0–2.5 μm within 20 dB dynamics. The SC generation includes two parts induced by DW (S_1) and soliton (S_2) as discussed in the above section. In the frequency domain, interference between S_1 and S_2 results in many peaks of intensity in a wavelength range of 1.45 – 1.65 μm, see Fig. 9 (b, d). In the time domain, although the SC is mainly induced by SPM and OWB, the anomalous dispersion

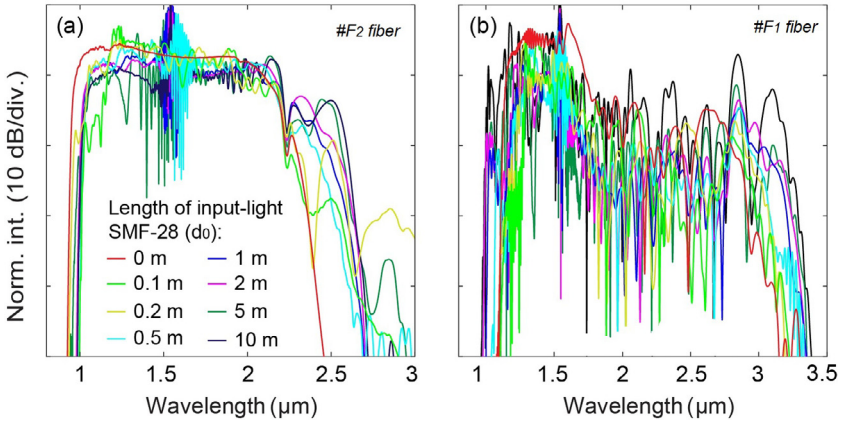

Fig. 10. Spectral bandwidth of SC generation in the proposed liquid core tapered fiber with various lengths of input-light SMF-28.

in the output-light untapered part (d_5) and output-light SMF-28 (d_6) leads to further delay of the leading edge, see Fig. 9(c).

Spectral bandwidth of SC generation induced in the liquid core fibers typically depends on the spectro-temporal properties of excitation pulses. For example, the ANDi SC generation is mainly induced in the waist part of $\#F_2$ fiber with contributions of SPM and OWB, in which OWB only occurs if there is temporal overlap between SMP-induced components and pulse tail (i.e., at 1.56 μm). Therefore, the spectral bandwidth of the ANDi SC generation solely depends on the amount of SPM-induced spectral broadening before OWB occurs. For a given peak power and dispersion shape, a bandwidth of SPM-induced spectral broadening is determined by the spectral position of a pump wavelength, meaning that a pump wavelength locates near ZDW (i.e., low value of dispersion) would offer further SPM-induced spectral bandwidth. For $\#F_1$ fiber, the spectral bandwidth of SC generation can be tuned by the central wavelength and pulse duration of excitation laser pulses via soliton fission and self-frequency shifting mechanism. This point implies that the spectral position of soliton (F), and thus, a length of input-light SMF-28 can trigger the spectral bandwidth of the SC generation in the liquid core fibers. As shown in Fig. 10, SC generation in both $\#F_1$ and $\#F_2$ fibers get broader spectral bandwidth by using a long length of the input-light SMF-28. In the other words, the spectral bandwidth of SC generation depends on the length of the input-light SMF-28. The use of a short length of the input-light SMF-28 (e.g., d_0 = 0.1 m or 0.2 m) does not provide efficiently broad spectral bandwidth because the input laser pulse does not significantly change during propagation in short sample SMF-28 via its low nonlinear coefficient.

3.4. SC generation with picosecond pulses

Supercontinuum generation induced by ultrashort laser pulses (sub-picosecond lasers) typically has broad-spectral spanning and high shot-to-shot coherence. Notwithstanding, there are remaining challenges related to the low spectral power densities (SPD) of these SC sources for specialized applications. For example, in multiphoton imaging techniques, a power spectral density (typically, above 2 mW/nm) requires for high-intensity of fluorescence signals and excellent sectioning effects [4]. However, the PSD of SC generated via femtosecond pulses lies below 0.5 mW/nm [4]. In fact, the SPD can be improved if pico and/or nanosecond lasers are used for SC generation.

It is worth noting that the nonlinearity of liquids (e.g., CS_2) depends on the pulse duration of excited lasers. For example, nonlinear refractive index of CS_2 via excitation of ultrashort laser pulses (FWHM < 100 fs) and picosecond pulses are around 3×10^{-19} m^2/W and 20×10^{-19} m^2/W, respectively [25]. The high nonlinearity enables broad SC generation via picosecond lasers in the investigated cascaded fibers. In addition, a noticeable feature of liquids that is significantly different from fiber glasses is an increase in Raman fraction (f_R) over laser pulse duration, such as f_R = 0.5 and f_R = 0.95 for excitation lasers with FWHM < 100 fs and FWHM ≈ 1 ps, respectively. The high value of Raman fraction leads to hybrid soliton dynamics in an anomalous dispersion regime, enabling a reduction of MI effects and an increase in shot-to-shot coherence [22].

Fig. 11 Presents picosecond-SC generation in cascaded fibers with $\#F_1$ and $\#F_2$. The excitation laser has a peak power of 27 kW (as a peak power used in the above sections) and a pulse duration of 1 ps. It is to note that the use of 1 ps pulse duration cases the significant spectral broadening in SMF-28 if a long sample of SMF-28 is used, such as d_0 = 1 m. The complex spectrogram in the input-light SMF-28 may cause a high error in the simulation of SC generation in the liquid-core tapered fiber by using the split-step method. Therefore, we only use a short length (d_0 = 10 cm) of input-light SMF-28 to significantly reduce the pulse distortion before launching it into the tapered liquid-core fibers.

The high value of Raman faction decreases soliton behaviors, meaning soliton shifting, and soliton fission (i.e., it takes a further length of nonlinear propagation for soliton fission) [22]. Therefore, SC generation in the cascaded fiber with $\#F_1$ is purely induced by SPM with spectral bandwidth from 1.1 μm to 2.3 μm, see Fig. 11 (a, b). The spectral bandwidth is narrower than that induced by the femtosecond laser with the same value of input peak power. SC generation with broad spectral bandwidth induced by SPM and soliton dynamics is possible to observe in a cascaded fiber with $\#F_1$ with a further length of the waist part (d_3). For instance, SC generation with a spectral bandwidth of 0.65 μm–3.3 μm in $\#F_1$ with d_3 = 5 cm is shown in Fig. 11 (c, d). In the case of cascaded fiber with $\#F_2$, nonlinear dynamics for spectral broadening are SPM and optical wave breaking at the trailing edge of the pulses, see Fig. 11 (e, f). As discussed in Section 3.3, optical wave breaking only occurs when there is temporal overlap between components of SPM-induced and pulse tail [62], therefore the increase in the waist length (d_3) does not significantly increase the spectral bandwidth of SC generation. Fig. 11 (g, h) presents ANDi SC generation in the cascaded fiber with $\#F_2$ (d_3 = 5 cm) with spectral spanning of 0.65 – 2.5 μm within 20 dB dynamics.

4. Conclusion

The cascaded fibers with tapered liquid fibers have been investigated for broad SC generation with the use of the femto and picosecond lasers at the C-band. The tapered process not only improves the nonlinear effects, but also modifies the dispersion, and thus, tuning the properties of nonlinear propagation. All tapered liquid core fibers have the same diameter of the input-light untapered part (d_1 = 14 μm) assuring high coupling efficiency with SMF-28 for a compact all-fiber system. With an input peak power of 27 kW, the cascaded fiber with $\#F_1$ provides anomalous dispersion SC generation with a spectral bandwidth of 1.0–3.3 μm within 30 dB dynamics, while cascaded fiber with

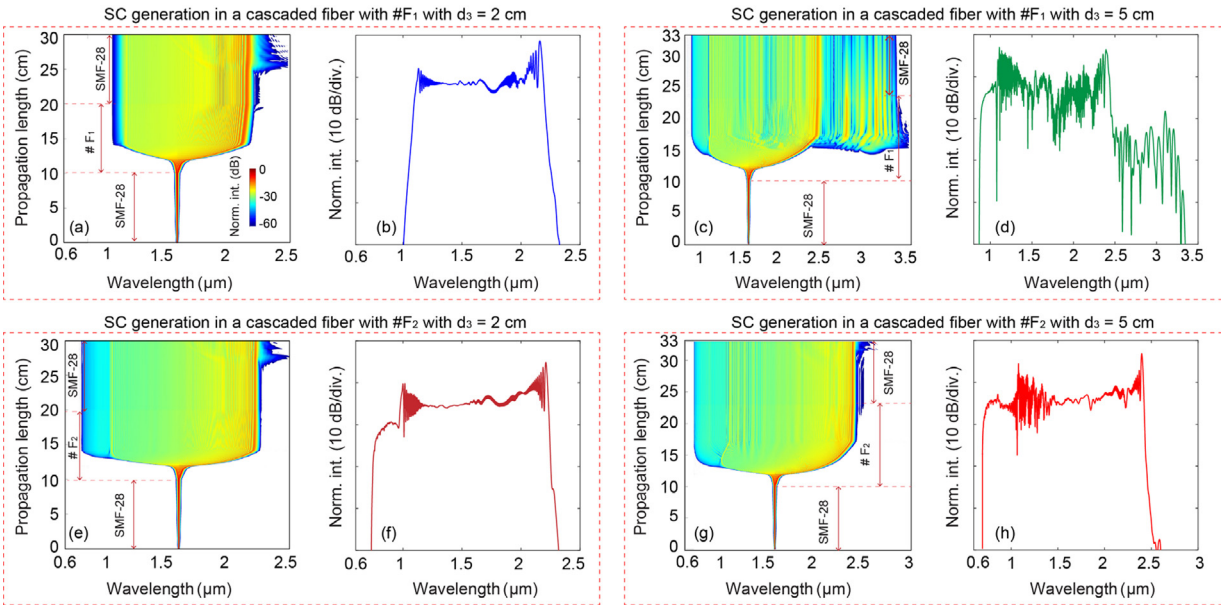

Fig. 11. SC generation and output spectrum in cascaded fibers with different length of the waist part. (a, b) $\#F_1$ with 2 cm waist length, (c, d) $\#F_1$ with 5 cm waist length, (e, f) $\#F_2$ with 2 cm waist length, (g, h) $\#F_2$ with 5 cm waist length. The laser has a peak power of 27 kW and 1 ps pulse duration.

$\#F_2$ offers ANDi SC generation with a spectral bandwidth of 1.0–2.5 μm within 20 dB dynamics.

The use of SMF-28 coupled with the tapered liquid-core fibers leads to slight modification in the temporal profile. In particular, the spectrogram includes the dispersive (S_1) and soliton (S_2) parts, in which the S_2 part mainly contributes to spectral broadening. In addition, the spectral bandwidth of SC generation can be broader if an appropriate length of SMF-28 is used for input-light coupling (d_0). It is to note that if further long SMF-28 is used, the laser pulse would be significantly starched out in the time domain, which reduces the peak power, and thus, decreases the spectral broadening.

Interestingly, directly launching the light into SMF-28 from the pump lasers (instead of directly coupling the light to the liquid-core fibers) is possible to mitigate the fiber damage and improve the stability of output SC spectra in long term. Therefore, a picosecond laser with high average power (average power of 800 mW, peak power of 27 kW) is used for SC generation. Although the SC generation is not broader than ones induced by femtosecond lasers, a high average input power, and thus, high spectral power density of output SC generation mat meet requirements for important applications in e.g., multiphoton microscopy, and LIDAR.

CRediT authorship contribution statement

Lanh Chu Van: Methodology, Writing – original draft, Funding acquisition. **Ngoc Vo Thi Minh:** Investigation. **Bao Tran Le Tran:** Investigation. **Trong Dang Van:** Investigation. **Phuong Nguyen Thi Hong:** Investigation. **Trang Do Mai:** Visualization. **Trung Le Canh:** Data curation. **Hieu Van Le:** Visualization. **Thuy Nguyen Thi:** Visualization. **Thanh Thai Doan:** Visualization. **Van Thuy Hoang:** Conceptualization, Methodology, Writing – original draft, Supervision, Writing – review & editing.

Declaration of competing interest

The authors declare that they have no known competing financial interests or personal relationships that could have appeared to influence the work reported in this paper.

Data availability

No data was used for the research described in the article.

Acknowledgment

This research is funded by Vietnam's Ministry of Education and Training (B2023-TDV-07).

References

[1] Marandi C.W., V.G. Rudy, E.M. Plotnichenko, K.L. Dianov, Vodopyanov, R.L. Byer, Mid-infrared supercontinuum generation in tapered chalcogenide fiber for producing octave-spanning frequency comb around 3μm, Opt. Express 20 (22) (2012) 24218–24225, http://dx.doi.org/10.1364/OE.20.024218.

[2] R.R. Alfano, The Supercontinuum Laser Source: The Ultimate White Light, third ed., Springer, New York, 2016.

[3] J.T. Woodward, A.W. Smith, C.A. Jenkins, C. Lin, S.W. Brown, K.R. Lykke, Supercontinuum sources for metrology, Metrologia 46 (4) (2009) S277, http://dx.doi.org/10.1088/0026-1394/46/4/S27.

[4] C. Poudel, C.F. Kaminski, Supercontinuum radiation in fluorescence microscopy and biomedical imaging applications, J. Opt. Soc. Am. B. 36 (2) (2019) A139–A153, http://dx.doi.org/10.1364/JOSAB.36.00A139.

[5] V.T. Hoang, Y. Boussafa, L. Sader, S. Février, V. Couderc, B. Wetzel, Optimizing supercontinuum spectro-temporal properties by leveraging machine learning towards multi-photon microscopy, Front. Photon. 3 (2022) 940902, http://dx.doi.org/10.3389/fphot.2022.940902.

[6] A.M. Heidt, J.M. Hodasi, A. Rampur, D. Spangenberg, M. Ryser, M. Klimczak, T. Feurer, Low noise all-fiber amplification of a coherent supercontinuum at 2μm and its limits imposed by polarization noise, Sci. Rep. 10 (2020) 16734, http://dx.doi.org/10.1038/s41598-020-73753-2.

[7] T. Sylvestre, E. Genier, A.N. Ghosh, P. Bowen, G. Genty, J. Troles, A. Mussot, A.C. Peacock, M. Klimczak, A.M. Heidt, J.C. Travers, O. Bang, J.M. Dudley, Recent advances in supercontinuum generation in specialty optical fibers, J. Opt. Soc. Am. B. 38 (12) (2021) F90–F103, http://dx.doi.org/10.1364/JOSAB.439330.

[8] B. Wetzel, M. Kues, P. Roztocki, C. Reimer, P. Godin, M. Rowley, B.E. Little, S.T. Chu, E.A. Viktorov, D.J. Moss, A. Pasquazi, M. Peccianti, R. Morandotti, Customizing supercontinuum generation via on-chip adaptive temporal pulse-splitting, Nature Commun. 9 (2018) 4884, http://dx.doi.org/10.1038/s41467-018-07141-w.

[9] G. Genty, L. Salmela, J.M. Dudley, D. Brunner, A. Kokhanovskiy, S. Kobtsev, S.K. Turitsyn, Machine learning and applications in ultrafast photonics, Nature Photon. 15 (2021) 91–101, http://dx.doi.org/10.1038/s41566-020-00716-4.

[10] A.I. Adamu, Md. S. Habib, C.R. Petersen, J.E.A. Lopez, B. Zhou, A. Schülzgen, M. Bache, R. Amezcua-Correa, O. Bang, C. Marko, Deep-UV to mid-IR supercontinuum generation driven by mid-IR ultrashort pulses in a gas-filled hollow-core fiber, Sci. Rep. 9 (2019) 4446, http://dx.doi.org/10.1038/s41598-019-39302-2.

[11] N. Kotsina, F. Belli, S. Gao, Y. Wang, P. Wang, J.C. Travers, D. Townsend, Ultrafast molecular spectroscopy using a hollow-core photonic crystal fiber light source, J. Phys. Chem. Lett. 10 (4) (2019) 715–720, http://dx.doi.org/10.1021/acs.jpclett.8b03777.

[12] J.C. Travers, T.F. Grigorova, C. Brahms, F. Belli, High-energy pulse self-compression and ultraviolet generation through soliton dynamics in hollow capillary fibres, Nature Photon. 13 (2019) 547–554, http://dx.doi.org/10.1038/s41566-019-0416-4.

[13] Z. Li, J.Yuan, C. Mei, F. Li, X. Zhou, B. Yan, Q. Wu, K. Wang, X. Sang, K. Long, C. Yu, Multi-octave mid-infrared supercontinuum and frequency comb generation in a suspended As2Se3 ridge waveguide, Appl. Opt. 58 (31) (2019) 8404–8410, http://dx.doi.org/10.1364/AO.58.008404.

[14] C.R. Petersen, U. Møller, I. Kubat, B. Zhou, S. Dupont, J. Ramsay, T. Benson, S. Sujecki, N. Abdel-Moneim, Z. Tang, D. Furniss, A. Seddon, Ole. Bang, Mid-infrared supercontinuum covering the 1.4–13.3μm molecular fingerprint region using ultra-high NA chalcogenide step-index fibre, Nature Photon. 8 (2014) 830–834, http://dx.doi.org/10.1038/nphoton.2014.213.

[15] H.V. Le, V.T. Hoang, G. Stępniewski, T.L. Canh, N.V.T. Minh, R. Kasztelanic, M. Klimczak, J. Pniewski, K.X. Dinh, A.M. Heidt, R. Buczyński, Low pump power coherent supercontinuum generation in heavy metal oxide solid-core photonic crystal fibers infiltrated with carbon tetrachloride covering 930–2500 nm, Opt. Express 29 (24) (2021) 39586–39600, http://dx.doi.org/10.1364/OE.443666.

[16] H.T. Tong, A. Koumura, A. Nakatani, H.P.T. Nguyen, M. Matsumoto, G. Sakai, T. Suzuki, Y. Ohishi, Chalcogenide all-solid hybrid microstructured optical fiber with polarization maintaining properties and its mid-infrared supercontinuum generation, Opt. Express 30 (14) (2022) 25433–25449, http://dx.doi.org/10.1364/OE.459745.

[17] L.C. Van, K.D. Xuan, T.L. Canh, T.T. Doan, T.N. Thi, H.V. Le, V.T. Hoang, Supercontinuum generation in chalcogenide photonic crystal fiber infiltrated with liquid, Opt. Mater. 137 (2023) 113547, http://dx.doi.org/10.1016/j.optmat.2023.113547.

[18] D.S. Shreesha Rao, L. Jensen, J.T. Grüner-Nielsen, P. Olsen, B. Heiduschka, J. Kemper, M. Schnekenburger, M. Glud, N.M. Mogensen, O. Israelsen, M. Bang, Shot-noise limited, supercontinuum-based optical coherence tomography, Light Sci. Appl. 10 (2021) 133, http://dx.doi.org/10.1038/s41377-021-00574-x.

[19] G. Zhou, et al., Design of supercontinuum laser hyperspectral light detection and ranging (LiDAR) (SCLaHS LiDAR), Int. J. Remote Sens. 42 (10) (2021) 3731–3755, http://dx.doi.org/10.1080/01431161.2021.1880662.

[20] S. Dai, Y. Wang, X. Peng, P. Zhang, X. Wang, Y. Xu, A review of mid-infrared supercontinuum generation in chalcogenide glass fibers, Appl. Sci. 8 (5) (2018) 707, http://dx.doi.org/10.3390/app8050707.

[21] V.T. Hoang, R. Kasztelanic, A. Anuszkiewicz, G. Stepniewski, A. Filipkowski, S. Ertman, D. Pysz, T. Wolinski, K.D. Xuan, M. Klimczak, R. Buczynski, All-normal dispersion supercontinuum generation in photonic crystal fibers with large hollow cores infiltrated with toluene, Opt. Mater. Express 8 (11) (2018) 3568–3582, http://dx.doi.org/10.1364/OME.8.003568.

[22] M. Chemnitz, M. Gebhardt, C. Gaida, F. Stutzki, J. Kobelke, J. Limpert, A. Tünnermann, M.A. Schmidt, Hybrid soliton dynamics in liquid-core fibres, Nature Commun. 8 (2018) 42, http://dx.doi.org/10.1038/s41467-017-00033-5.

[23] V.T. Hoang, R. Kasztelanic, G. Stępniewski, K.D. Xuan, V.C. Long, M. Trippenbach, M. Klimczak, R. Buczyński, J. Pniewski, Femtosecond supercontinuum generation around 1560 nm in hollow-core photonic crystal fibers filled with carbon tetrachloride, Appl. Opt. 59 (12) (2020) 3720–3725, http://dx.doi.org/10.1364/AO.385003.

[24] M. Reichert, H. Hu, M.R. Ferdinandus, M. Seidel, P. Zhao, T.R. Ensley, D. Peceli, J.M. Reed, D.A. Fishman, S. Webster, D.J. Hagan, E.W. Van Stryland, Temporal, spectral, and polarization dependence of the nonlinear optical response of carbon disulfide, Optica 1 (6) (2014) 436–445, http://dx.doi.org/10.1364/OPTICA.1.000436.

[25] P. Zhao, M. Reichert, S. Benis, D.J. Hagan, E.W.V. Stryland, Temporal and polarization dependence of the nonlinear optical response of solvents, Optica 5 (5) (2018) 583–594, http://dx.doi.org/10.1364/OPTICA.5.000583.

[26] S. Junaid, W. Huang, R. Scheibinger, K. Schaarschmidt, H. Schneidewind, P. Paradis, M. Bernier, R. Vallée, S. Stanca, G. Zieger, M.A. Schmidt, Attenuation coefficients of selected organic and inorganic solvents in the mid-infrared spectral domain, Opt. Mater. Express 12 (4) (2022) 1754–1763, http://dx.doi.org/10.1364/OME.455405.

[27] H.L. Van, V.T. Hoang, T.L. Canh, Q.H. Dinh, H.T. Nguyen, N.V.T. Minh, M. Klimczak, R. Buczynski, R. Kasztelanic, Silica-based photonic crystal fiber infiltrated with 1, 2-dibromoethane for supercontinuum generation, Appl. Opt. 60 (24) (2021) 7268–7278, http://dx.doi.org/10.1364/AO.430843.

[28] L.C. Van, B.T.L. Tran, T.D. Van, N.V.T. Minh, T.N. Thi, H.P.N. Thi, M.H.T. Nguyen, V.T. Hoang, Supercontinuum generation in highly birefringent fiber infiltrated with carbon disulfide, Opt. Fiber Technol., Mater. Devices Syst. 75 (2023) 103151, http://dx.doi.org/10.1016/j.yofte.2022.103151.

[29] M. Chemnitz, R. Scheibinger, C. Gaida, M. Gebhardt, F. Stutzki, S. Pumpe, J. Kobelke, A. Tünnermann, J. Limpert, M.A. Schmidt, Thermodynamic control of soliton dynamics in liquid-core fibers, Optica 5 (6) (2018) 695–703, http://dx.doi.org/10.1364/OPTICA.5.000695.

[30] L.C. Van, V.T. Hoang, V.C. Long, K. Borzycki, K.D. Xuan, V.T. Quoc, M. Trippenbach, R. Buczynski, J. Pniewski, Supercontinuum generation in benzene-filled hollow-core fibers, Opt. Eng. 60 (11) (2021) 116109, http://dx.doi.org/10.1117/1.OE.60.11.116109.

[31] M. Chemnitz, C. Gaida, M. Gebhardt, F. Stutzki, J. Kobelke, A. Tünnermann, J. Limpert, M.A. and Schmidt, Carbon chloride-core fibers for soliton mediated supercontinuum generation, Opt. Express 26 (3) (2018) 3221–3235, http://dx.doi.org/10.1364/OE.26.003221.

[32] S. Junaid, J. Bierlich, A. Hartung, T. Meyer, M. Chemnitz, M.A. Schmidt, Supercontinuum generation in a carbon disulfide core microstructured optical fiber, Opt. Express 29 (13) (2021) 19891–19902, http://dx.doi.org/10.1364/OE.426313.

[33] H.V. Le, V.T. Hoang, H.T. Nguyen, V.C. Long, R. Buczynski, R. Kasztelanic, Supercontinuum generation in photonic crystal fibers infiltrated with tetrachloroethylene, Opt. Quantum Electron 53 (2021) 187, http://dx.doi.org/10.1007/s11082-021-02820-3.

[34] D. Marcuse, Loss analysis of single-mode fiber splices, Bell Labs Tech.J. 56 (5) (1977) 703–718, http://dx.doi.org/10.1002/j.1538-7305.1977.tb00534.x.

[35] V.T. Hoang, R. Kasztelanic, A. Filipkowski, G. Stępniewski, D. Pysz, M. Klimczak, S. Ertman, V.C. Long, T.R. Woliński, M. Trippenbach, K.D. Xuan, M. Śmietana, R. Buczyński, Supercontinuum generation in an all-normal dispersion large core photonic crystal fiber infiltrated with carbon tetrachloride, Opt. Mater. Express 9 (5) (2019) 2264–2278, http://dx.doi.org/10.1364/OME.9.002264.

[36] Y. Zhang, J. Yuan, K. Wang, H. Wang, Y. Cheng, C. Mei, F. Xu, X. Zhou, B. Yan, X. Sang, C. Yu, Cascaded-tapered silica photonic crystal fiber for supercontinuum generation, Opt. Eng. 59 (12) (2020) 126107, http://dx.doi.org/10.1117/1.OE.59.12.126107.

[37] T.A. Birks, W.J. Wadsworth, P. St. J. Russell, Supercontinuum generation in tapered fibers, Opt. Lett. 25 (19) (2000) 1415–1417, http://dx.doi.org/10.1364/OL.25.001415.

[38] N. Zhang, X. Peng, Y. Wang, S. Dai, Y. Yuan, J. Su, G. Li, P. Zhang, P. Yang, X. Wang, Ultrabroadband and coherent mid-infrared supercontinuum generation in te-based chalcogenide tapered fiber with all-normal dispersion, Opt. Express 27 (7) (2019) 10311–10319, http://dx.doi.org/10.1364/OE.27.010311.

[39] M.I. Suresh, J. Hammer, N.Y. Joly, J. St, P. Russell, F. Tani, Deep-UV-enhanced supercontinuum generated in a tapered gas-filled photonic crystal fiber, Opt. Lett. 46 (18) (2021) 4526–4529, http://dx.doi.org/10.1364/OL.435697.

[40] T.S. Saini, T.H. Tuan, T. Suzuki, Y. Ohishi, Coherent mid-ir supercontinuum generation using tapered chalcogenide step-index optical fiber: experiment and modelling, Sci. Rep. 10 (2020) 2236, http://dx.doi.org/10.1038/s41598-020-59288-6.

[41] A. Hartung, A.M. Heidt, H. Bartelt, Pulse-preserving broadband visible supercontinuum generation in all-normal dispersion tapered suspended-core optical fibers, Opt. Express 19 (13) (2011) 12275–12283, http://dx.doi.org/10.1364/OE.19.012275.

[42] V.T. Hoang, B. Siwicki, M. Franczyk, G. Stępniewski, H.L. Van, V.C. Long, M. Klimczak, R. Buczyński, Broadband low-dispersion low-nonlinearity photonic crystal fiber dedicated to near-infrared high-power femtosecond pulse delivery, Opt. Fiber Technol., Mater. Devices Syst. 42 (2018) 119–125, http://dx.doi.org/10.1016/j.yofte.2018.03.003.

[43] NKT Photonics, https://www.nktphotonics.com/products/optical-fibers-and-modules/large-mode-area-photonic-crystal-fibers/.

[44] T.A. Birks, Y.W. and Li, The shape of fiber tapers, J. Lightwave Technol. 10 (4) (1992) 432–438, http://dx.doi.org/10.1109/50.134196.

[45] S. Pricking, H. Giessen, Tapering fibers with complex shape, Opt. Express 18 (4) (2010) 3426–3437, http://dx.doi.org/10.1364/OE.18.003426.

[46] H.C. Nguyen, B.T. Kuhlmey, E.C. Magi, M.J. Steel, P. Domachuk, C.L. Smith, B.J. Eggleton, Tapered photonic crystal fibres: properties, characterisation and applications, Appl. Phys. B 81 (2005) 377–387, http://dx.doi.org/10.1007/s00340-005-1901-7.

[47] A. Felipe, G. Espíndola, H.J. Kalinowski, J.A.S. Lima, A.S. Paterno, Stepwise fabrication of arbitrary fiber optic tapers, Opt. Express 20 (18) (2012) 19893–19904, http://dx.doi.org/10.1364/OE.20.019893.

[48] M. Liao, W. Gao, Z. Duan, X. Yan, Directly draw highly nonlinear tellurite microstructured fiber with diameter varying sharply in a short fiber length, Opt. Express 20 (2) (2012) 1141–1150, http://dx.doi.org/10.1364/OE.20.001141.

[49] S. Kedenburg, T. Gissibl, T. Steinle, A. Steinmann, H. Giessen, Towards integration of a liquid-filled fiber capillary for supercontinuum generation in the 1.2–2.4μm range, Opt. Express 23 (7) (2015) 8281–8289, http://dx.doi.org/10.1364/OE.23.008281.

[50] K. Kieu, L. Schneebeli, R.A. Norwood, N. Peyghambarian, Integrated liquid-core optical fibers for ultra-efficient nonlinear liquid photonics, Opt. Express 20 (7) (2012) 8148–8154, http://dx.doi.org/10.1364/OE.20.008148.

[51] Heraeus, Heraeus https://www.heraeus.com/en/group/home/home.html.

[52] D. Mogilevtsev, T.A. Birks, P. St. J. Russell, Group-velocity dispersion in photonic crystal fibers, Opt. Lett. 23 (21) (1998) 1662–1664, http://dx.doi.org/10.1364/OL.23.001662.

[53] K. Saitoh, N. Florous, M. Koshiba, Ultra-flattened chromatic dispersion controllability using a defected-core photonic crystal fiber with low confinement losses, Opt. Express 13 (21) (2005) 8365–8371, http://dx.doi.org/10.1364/OPEX.13.008365.

[54] F. Poletti, P. Horak, Dynamics of femtosecond supercontinuum generation in multimode fibers, Opt. Express 17 (8) (2009) 6134–6147, http://dx.doi.org/10.1364/OE.17.006134.

[55] I. Kubat, O. Bang, Multimode supercontinuum generation in chalcogenide glass fibres, Opt. Express 24 (3) (2016) 2513–2526, http://dx.doi.org/10.1364/OE.24.002513.

[56] P.D. Drummond, J.F. Corney, Quantum noise in optical fibers. I. Stochastic equations, J. Opt. Soc. Amer. B 18 (2) (2001) 139–152, http://dx.doi.org/10.1364/JOSAB.18.000139.

[57] E. Genier, P. Bowen, T. Sylvestre, J.M. Dudley, P. Moselund, O. Bang, Amplitude noise and coherence degradation of femtosecond supercontinuum generation in all-normal-dispersion fibers, J. Opt. Soc. Amer. B 36 (2) (2019) A161–A167, http://dx.doi.org/10.1364/JOSAB.36.00A161.

[58] L.C. Van, T.N. Thi, B.T.L. Tran, D.H. Trong, N.V.T. Minh, H.V. Le, V.T. Hoang, Multi-octave supercontinuum generation in As2Se3 chalcogenide photonic crystal fiber, Phot. Nanostruct. Fundam. Appl. 48 (2022) 100986, http://dx.doi.org/10.1016/j.photonics.2021.100986.

[59] MenloSystem, https://www.menlosystems.com/products/femtosecond-lasers-and-amplifiers/elmo/.

[60] J.M. Dudley, G. Genty, S. Coen, Supercontinuum generation in photonic crystal fiber, Rev. Modern Phys. 78 (2006) 1135, http://dx.doi.org/10.1103/RevModPhys.78.1135.

[61] C. Mei, G. Steinmeyer, J. Yuan, X. Zhou, K. Long, Intermodal synchronization effects in multimode fibers with noninstantaneous nonlinearity, Phys. Rev. A 105 (2022) 013516, http://dx.doi.org/10.1103/PhysRevA.105.013516.

[62] A.M. Heidt, A. Hartung, G.W. Bosman, P. Krok, E.G. Rohwer, H. Schwoerer, H. Bartelt, Coherent octave spanning near-infrared and visible supercontinuum generation in all-normal dispersion photonic crystal fibers, Opt. Express 19 (4) (2011) 3775–3787, http://dx.doi.org/10.1364/OE.19.003775.